# Catalysis Science & Technology

rsc.li/catalysis

ROYAL SOCIETY
OF **CHEMISTRY**

**PAPER**
Ulrich Hintermair *et al.*
Mapping catalyst activation, turnover speciation and
deactivation in Rh/PPh$_3$-catalysed olefin hydroformylation

Check for updates

# Mapping catalyst activation, turnover speciation and deactivation in Rh/PPh₃-catalysed olefin hydroformylation†

Alejandro Bara-Estaún, [iD] [ab] Catherine L. Lyall, [iD] [ab] John P. Lowe, [iD] [ab] Paul G. Pringle, [iD] [d] Paul C. J. Kamer, [iD] [e] Robert Franke[fg] and Ulrich Hintermair [iD] ★[abc]

We report new insights into the fate of the precious metal during hydroformylation catalysis of 1-hexene with Rh/PPh₃ complexes using multi-nuclear *operando* FlowNMR spectroscopy. By applying selectively excited ¹H and ³¹P{¹H} NMR pulse sequences we were able to characterise and quantify key hydrido-rhodium and acyl-rhodium intermediates formed during turnover as well as dormant dimeric carbonyl complexes. The quantitative catalyst distribution maps derived this way explain catalyst stability and activity across a range of reaction conditions, including why CO-lean conditions give faster hydroformylation catalysis through the suppression of dimer and cluster formation. The activation behaviour of five commonly used precursors and the thermal stability of the phosphine-hydrido complex [RhH(CO)(PPh₃)₃] have been investigated, and the benefits of applying controlled temperature gradients for quantitative FlowNMR spectroscopic reaction monitoring of dynamic catalyst systems are demonstrated.

## 1 Introduction

The reaction in which aldehydes are formed from olefins with H₂ and CO in the presence of a suitable catalyst is known as hydroformylation or the "oxo" process.[1] Originally discovered by Otto Roelen in 1938,[2] it has since been studied extensively in both industrial and academic settings with a variety of ligands and metals.[3,4] Rh and Co stand out as hydroformylation catalysts as, to date, they are still the only ones used in industry due to their high selectivity and activity.[5] Nowadays, catalytic hydroformylation of olefins mediated by cobalt or rhodium complexes is one of the largest and most important industrial applications of homogeneous catalysis with an annual production of over 10 million metric tonnes in 2008.[6] A large proportion of contemporary hydroformylation processes use the more active rhodium catalysts with phosphine or phosphite ligands in organic or aqueous/organic solution.[7,8] New insights regarding the structure and catalytic relevance of various reaction intermediates have been discovered thanks to the development of new spectroscopic and computational techniques.[6] Nevertheless, the elevated pressure and temperature used in addition to the O₂ sensitivity of the catalysts still pose a challenge for true *operando* studies.[9] Initial rate kinetic analyses and *in situ* IR and NMR studies have shed some light on the reaction mechanism and identified [RhH(CO)₂(PPh₃)₂] as the dominant catalyst state,[10] but a quantitative picture of the catalyst speciation during activation and turnover is still lacking. Furthermore, the fate of dormant off-cycle species and catalyst decomposition pathways, knowledge crucial to commercial processes using an expensive noble metal such as rhodium, has received little attention.[6]

IR spectroscopy has long been the technique of choice for investigating hydroformylation catalysts due to the strong, characteristic absorptions of carbonyl functionalities. Since the development of high-pressure IR (HP-IR) cells, different setups have been designed and used in carbonylation chemistry.[11–13] A recent example was reported by Selent *et al.*, who designed a bespoke *in situ* HP-IR autoclave especially suited for *operando* mechanistic studies.[14] IR spectroscopy is a fast and sensitive analytical technique, but it provides

*a Department of Chemistry, University of Bath, Claverton Down, BA2 7AY Bath, UK.*
*E-mail: uh213@bath.ac.uk*
*b Dynamic Reaction Monitoring Facility, University of Bath, Claverton Down, BA2 7AY Bath, UK*
*c Centre for Sustainable & Circular Technologies, University of Bath, Bath BA2 7AY, UK*
*d School of Chemistry, University of Bristol, Cantock's Close, Bristol BS8 1TS, UK*
*e Leibniz Institute for Catalysis, Albert-Einstein-Straße 29A, 18059 Rostock, Germany*
*f Evonik Performance Materials GmbH, Paul-Baumann-Straße 1, 45772 Marl, Germany*
*g Lehrstuhl für Theoretische Chemie, Ruhr-Universität Bochum, 44780 Bochum, Germany*
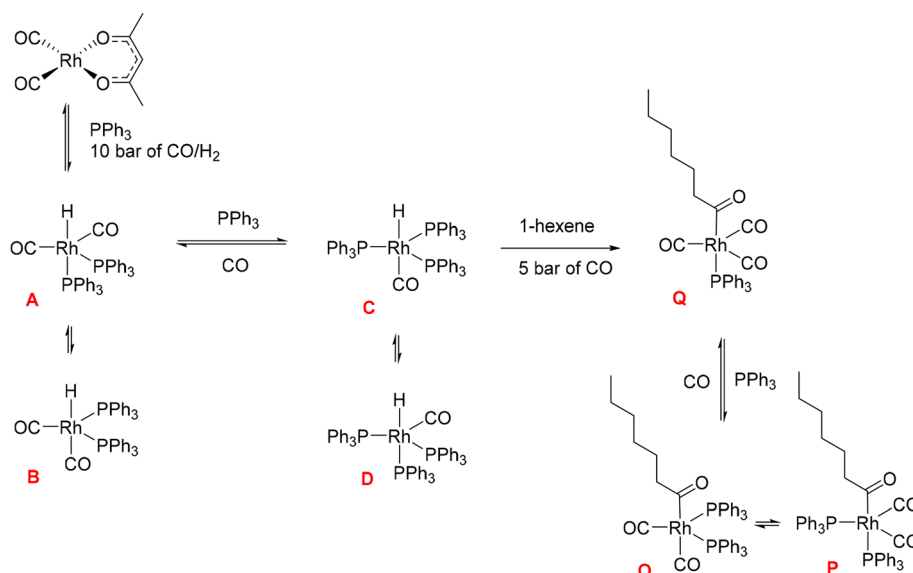
† Electronic supplementary information (ESI) available. See DOI: https://doi.org/10.1039/d2cy00312k

This journal is © The Royal Society of Chemistry 2022

*Catal. Sci. Technol.*, 2022, **12**, 5501–5516 | 5501

limited structural information and is often only used qualitatively due to the need for individual peak calibration. Despite being a slower and less sensitive technique than IR, NMR spectroscopy provides inherently quantitative data, offers wide applicability due to the number of NMR active nuclei, and provides detailed information on molecular structure and dynamics.[15] Previously, *in situ* NMR studies on Rh/PR$_3$ hydroformylation systems have been carried out in static high-pressure NMR tubes using $^{31}$P NMR experiments.[16] However, the absence of active mixing and associated mass transfer limitations (in particular gas depletion) mean that observations derived from such experiments are of limited relevance to real-world process conditions.[17] Online multi-nuclear high resolution FlowNMR spectroscopy has recently been shown to be a suitable technique to perform *operando* studies of complex reaction mixtures during catalytic turnover.[18] When flow effects on signal quantification are accounted for[18] and engineering aspects of the flow system considered,[19] accurate data on the reaction progress and catalyst speciation free from mass transport limitations may be obtained even for highly air-sensitive systems operating at elevated temperature and pressure.[20–23] FlowNMR has also been used to monitor the amount of H$_2$ dissolved in solution at low[24] and high pressures[25] after consideration of flow effects and the *ortho/para* ratio of H$_2$.

Hydroformylation reactions have been studied by *operando* FlowNMR spectroscopy as well. Burés *et al.* reported a kinetic study of an Rh/phosphite-catalysed hydroformylation reaction in 2019, but without any catalyst characterisation.[26] In the same year, Landis *et al.* published a detailed kinetic analysis of an asymmetric Rh-catalysed hydroformylation studied using a 10 mm high-pressure sample tube as a stationary reactor in the NMR spectrometer with active gas and liquid recirculation.[27] They developed a microkinetic model for Rh(bis-diazaphospholane)-catalysed hydroformylation that fit catalytic and stoichiometric reaction data well. In 2020 we reported an investigation of the Rh/PPh$_3$ catalysed hydroformylation of 1-hexene by multi-nuclear, high pressure, *operando* FlowNMR spectroscopy.[28] $^1$H NMR experiments together with selectively excited $^1$H NMR and $^{31}$P{$^1$H} NMR pulse sequences were interleaved to monitor the reaction. $^1$H NMR data allowed the quantification of dissolved H$_2$ while tracking substrate consumption and product formation to obtain high-quality reaction progress profiles. Selectively excited $^1$H and $^{31}$P{$^1$H} NMR experiments in combination with diffusion measurements and 2D NMR experiments were used to detect Rh/PPh$_3$ intermediates during catalytic turnover (Scheme 1). The isomeric *e,a* and *e,e* bis-phosphine complexes [RhH(CO)$_2$(PPh$_3$)$_2$] (**A/B**) were observed as the predominant hydrido phosphine Rh complex during turnover. They formed reversibly from the isomeric *e,e,e* and *e,e,a* tris-phosphine complexes [RhH(CO)(PPh$_3$)$_3$] (**C/D**) under CO pressure, or directly from [Rh(acac)(CO)$_2$] with excess PPh$_3$ under H$_2$ and CO. The mono-phosphine *trans*-acyl complex [Rh(CO(CH$_2$)$_5$CH$_3$)(CO)$_3$(PPh$_3$)] (**Q**), in equilibrium with the *e,e* and *e,a* bis-phosphine acyl complexes [Rh(CO(CH$_2$)$_5$CH$_3$)(CO)$_2$(PPh$_3$)$_2$] (**O/P**), was characterised as an in-cycle species prior to hydrogenolysis that liberates the aldehyde product when using two or less equivalents of PPh$_3$ in the reaction. These acyl complexes could also be obtained by mixing 1-hexene with **C/D** under an atmosphere of CO without H$_2$ present.

Initially, these Rh species have not been quantified due to low signal-to-noise (S/N) caused by flow effects and their fluxional behaviour as a result of various intra- and inter-molecular exchange processes under the reaction conditions. The $^{31}$P{$^1$H} NMR signal for the excess free PPh$_3$ was



**Scheme 1** Phosphine Rh complexes detected and characterised by FlowNMR spectroscopy when monitoring the hydroformylation of 1-hexene in the presence of Rh(acac)(CO)$_2$/PPh$_3$ at 50 °C in toluene.[28]

**5502** | *Catal. Sci. Technol.*, 2022, **12**, 5501–5516

This journal is © The Royal Society of Chemistry 2022

sometimes broadened to the limit of detection and scalar P–H, Rh–H and C–P couplings obscured by the fast interconversion of multiple species. Here we report methods to make $^{31}P\{^1H\}$ NMR and selective excitation $^1H$ NMR measurements robustly quantitative in flow in order to map the distribution of catalytic intermediates before, during and after turnover. Besides building a more comprehensive picture of the mechanism of Rh/PR$_3$-catalysed hydroformylation, our results yield important insights into unproductive off-cycle species relevant for efficient application with optimum use of the precious metal.

## 2 Results and discussion

### 2.1 NMR signal quantification

The accurate quantification of NMR signals (qNMR) requires careful selection of acquisition parameters, such as spectral width (SW), transmitter excitation frequency (O$^1$P), number of scans (NS), digital resolution (sampling rate), and the intercorrelated choice of flip angle (FA) and acquisition (AQ) plus delay $(D_1)$ time.[29–32] Once these settings have been optimised, a critical parameter of the analyte(s) under investigation are the longitudinal or spin–lattice relaxation time constants $(T_1)$ of the nuclei of interest, as the $D_1$ of the NMR experiment must be at least five times the longest $T_1$ to give a quantitative NMR signal.[30] $T_1$ values for $^1H$ and $^{31}P$ in medium-sized molecules may vary from 0.1 s to 20 s, a considerable range that can greatly affect signal quantification. These values are often not known *a priori* and are difficult to tabulate as they vary with temperature,
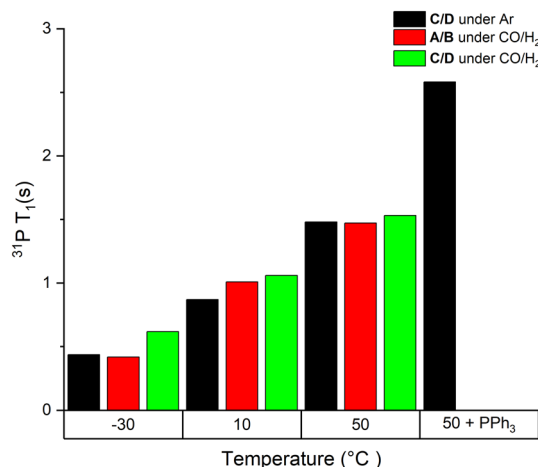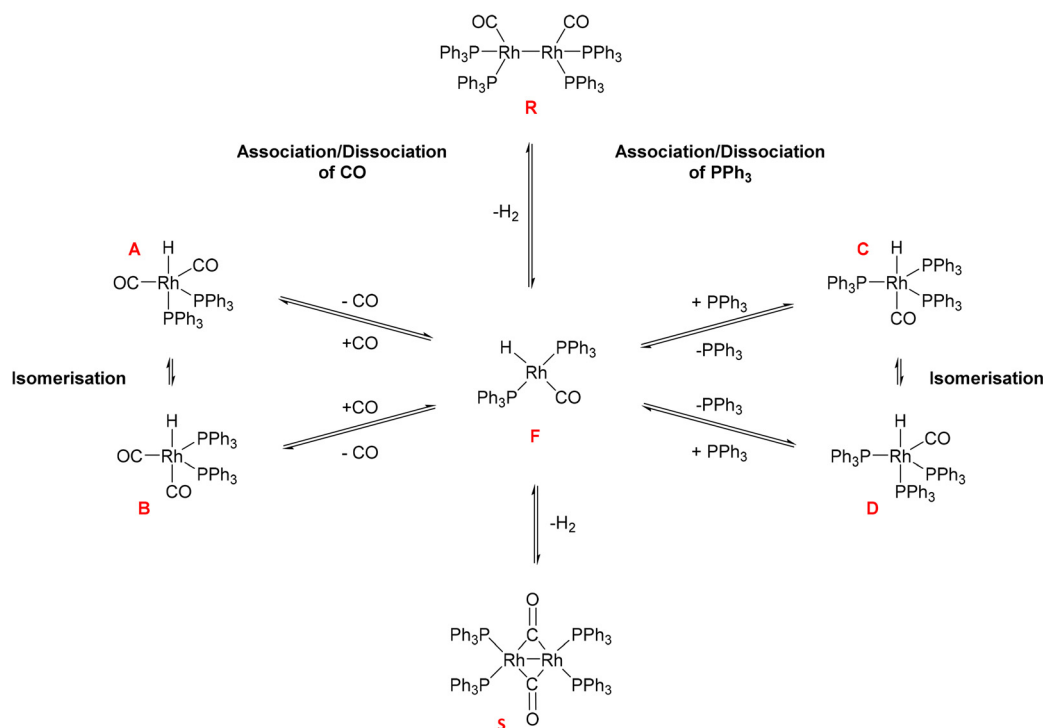


**Fig. 1** Static $^{31}P$ $T_1$ values of mixtures of complexes **A/B** and **C/D** at 40 mM in toluene under different conditions as indicated.

solvent, matrix of reaction mixture and even gas composition.[33] In continuous flow, signal quantification is further complicated by flow effects, making the absolute quantification of FlowNMR data critically dependant on careful calibration against static spectra (or precise knowledge of all relevant $T_1$ values) and the use of an internal standard.[28] In our previous work[28] all $^1H$ FlowNMR data, including selective excitation experiments, had been made quantitative in this way, but any $^{31}P\{^1H\}$ FlowNMR observations remained qualitative due to the absence of a $^{31}P$ NMR standard, unknown range of $T_1^*$ values and broadened signals. In the following we address these limitations.



**Scheme 2** Exchange equilibria between **A/B** and **C/D** in the presence of syngas and excess PPh$_3$ (dimers **R** and **S** will be discussed in more detail below; **F** has not been observed experimentally).

This journal is © The Royal Society of Chemistry 2022

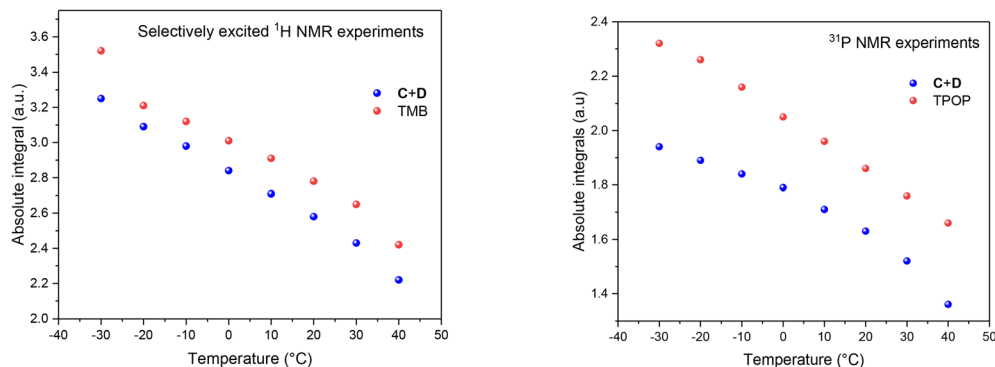*Catal. Sci. Technol.*, 2022, **12**, 5501–5516 | **5503**

**Fig. 2** Absolute integral of **C/D** and TMB obtained from selective excitation $^1$H NMR spectroscopy (left) and absolute integral of **C/D** and TPOP obtained from $^{31}$P{$^1$H} NMR spectroscopy (right) of a non-deuterated toluene solution containing 45 mM [RhH(CO)(PPh$_3$)$_3$], 10 mM of trimethoxybenzene and 10 mM of triphenylorthophosphate under argon.

**2.1.1 $^{31}$P $T_1$ characterisation and exchange effects.** To get an idea of the range of $^{31}$P $T_1$ values in typical hydroformylation intermediates under reaction conditions, we measured the spin–lattice relaxation time constants of [RhH(CO)(PPh$_3$)$_3$] (**C/D**) and [RhH(CO)$_2$(PPh$_3$)$_2$] (**A/B**) at different temperatures, under syngas and argon, and with excess of free PPh$_3$ *via* inversion recovery experiments in static, high-pressure NMR sample tubes (Fig. 1).[34]

As can be seen from the data in Fig. 1, $T_1$ values of the bound PPh$_3$ in both Rh complexes were relatively short (<3 s) but increased three-fold when increasing the temperature from −30 °C to 50 °C. We found less than 15% difference between the two complexes at any point, which is likely due to their similar structure and comparable degree of fluxionality. The effect of syngas *versus* argon was similarly small, indicating a negligible effect of excess CO (causing interconversion between **A/B** and **C/D**) on the quantification of either complex. However, the addition of excess PPh$_3$ to **C/D** almost doubled the $T_1$ value of Rh-bound PPh$_3$ ligand. This is likely a mixing effect that depends on the residence time of the ligand on the metal as well as the respective relaxation time constants of the bound and free state of the ligand, highlighting the difficulty of accurate $^{31}$P NMR quantification of such dynamic mixtures (Scheme 2). This impact of free ligand on signal quantification is especially relevant to hydroformylation chemistry where different amounts of ligand excess are often compared. Nevertheless, measuring the $T_1$ values under the reaction conditions applied or using appropriately long $D_1$ times allows for precise signal quantification.

**2.1.2 Use of multiple internal standards.** 1,3,5-Trimethoxybenzene (TMB) has proven to be a useful internal standard for $^1$H measurements in previous FlowNMR studies.[24] For $^{31}$P quantification we found triphenylorthophosphate (TPOP) to be suitable, as it did not interact with the catalytic system while providing a well-resolved, separate $^{31}$P{$^1$H} NMR signal without undue spectral crowding of the $^1$H domain. Note that the static $^{31}$P{$^1$H} NMR calibration spectra should use inverse-gated decoupling to prevent signal enhancement through NOEs (nuclear

overhauser effect).[34] To test the validity and accuracy of the two internal standards we compared the $^1$H and $^{31}$P signal quantification of molecules which contained both functionalities. Using the Wilkinson complex **C/D** in a high-pressure NMR tube with known amounts of both TMB and TPOP in non-deuterated toluene we carried out a series of selectively excited $^1$H and quantitative $^{31}$P{$^1$H} NMR experiments at different temperatures using the above-determined $T_1$ values (Fig. 1). The absolute integral data for the Rh complex **C/D** against the two internal standards at different temperatures are shown in Fig. 2. The most obvious observation that all signal intensities increased with decreasing temperature (Fig. S1†) is due to the Maxwell–Boltzmann distribution of the $I = \frac{1}{2}$ nuclei between the two magnetic states.[35]

The fact that the signal intensities of both standards paralleled the signal intensities of the $^1$H and $^{31}$P NMR signals of the dynamic complex [RhH(CO)(PPh$_3$)$_3$] (Scheme 2) over a range of 70 °C suggests that although the compound engages in both intramolecular and intermolecular exchange processes, it may be accurately quantified using either



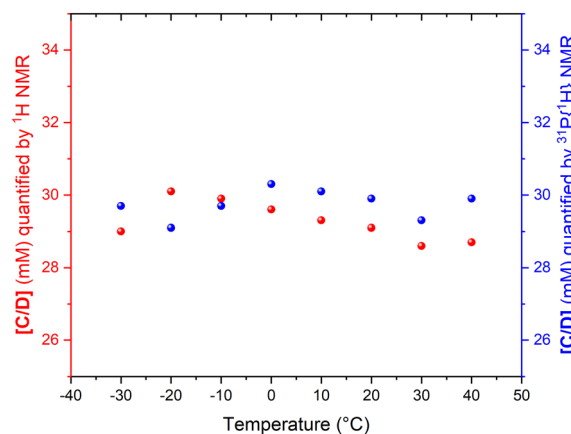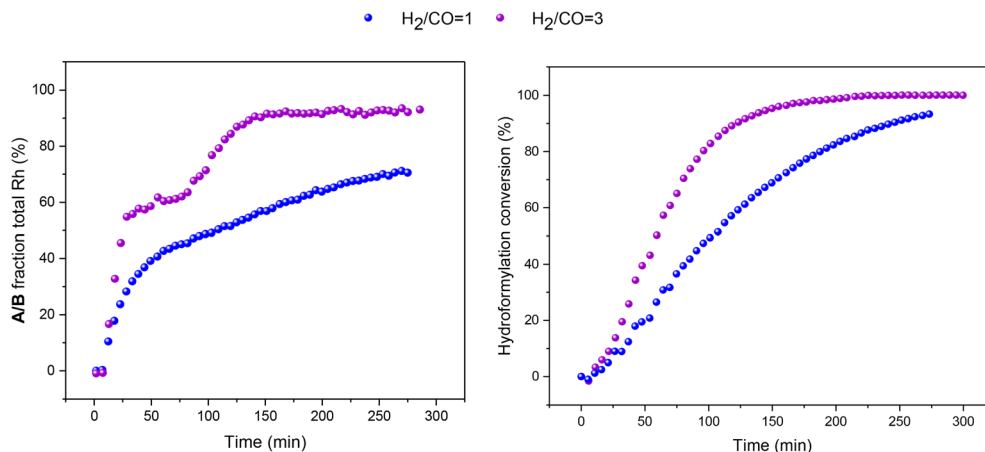**Fig. 3** Concentration of **C/D** quantified by selective excitation $^1$H and $^{31}$P{$^1$H} NMR spectroscopy in the mixture containing 40 mM of [RhH(CO)(PPh$_3$)$_3$], 10 mM of TMB and 10 mM of TPOP in 0.8 mL of non-deuterated toluene under argon.

**Fig. 4** Reaction conditions of the hydroformylation of 1-hexene (upper) and schematic of the FlowNMR apparatus (lower).

nucleus as long as their NMR signals do not decoalesce. This assertion is further supported by the direct comparison of both integral values against their respective internal standards which do not engage in any dynamic exchanges (Fig. 3).

As the data in Fig. 3 shows, with suitable acquisition parameters both nuclei allow accurate quantification of the same complex against either standard over a range of temperatures, cancelling out the effect of a shift in the Boltzmann distribution (visible in Fig. 2). When the experiment was repeated under 5 bar of syngas, conditions that cause **C**/**D** to engage in additional exchange equilibria (Scheme 2), the quantification of **C**/**D** against either internal

standard remained accurate although new (separate) signals for **A**/**B** were observed (Fig. S2–S4†). Dilution down to catalytic loadings of Rh did not affect the validity of the signal quantification either (Fig. S5†), showing the quantification method to extend robustly to process conditions.

## 2.2 Hydroformylation of 1-hexene catalysed by [Rh(acac)-(CO)$_2$] + PPh$_3$

The hydroformylation of 1-hexene in the presence of [Rh(acac)(CO)$_2$] and various amounts of PPh$_3$ was studied by quantitative $^1$H, selective excitation $^1$H and $^{31}$P{$^1$H} FlowNMR



**Fig. 5** Amount of **A**/**B** detected by quantitative $^1$H FlowNMR spectroscopy during hydroformylation of 1-hexene under 12 bar of CO/H$_2$ (1 : 1) at 50 °C catalysed by [Rh(acac)(CO)$_2$] = 2.5 mM and [PPh$_3$] = 7.5, 15, 25 and 50 mM in 22.4 mL of non-deuterated toluene *versus* conversion over time.

**Fig. 6** Amount of **A/B** detected by quantitative $^1$H FlowNMR spectroscopy during hydroformylation of 1-hexene under 12 bar of CO/H$_2$ (1:1) at 50 °C catalysed by [Rh(acac)(CO)$_2$] = 2.5 mM and [PPh$_3$] = 7.5, 15, 25 and 50 mM in 22.4 mL of non-deuterated toluene *versus* conversion over time.
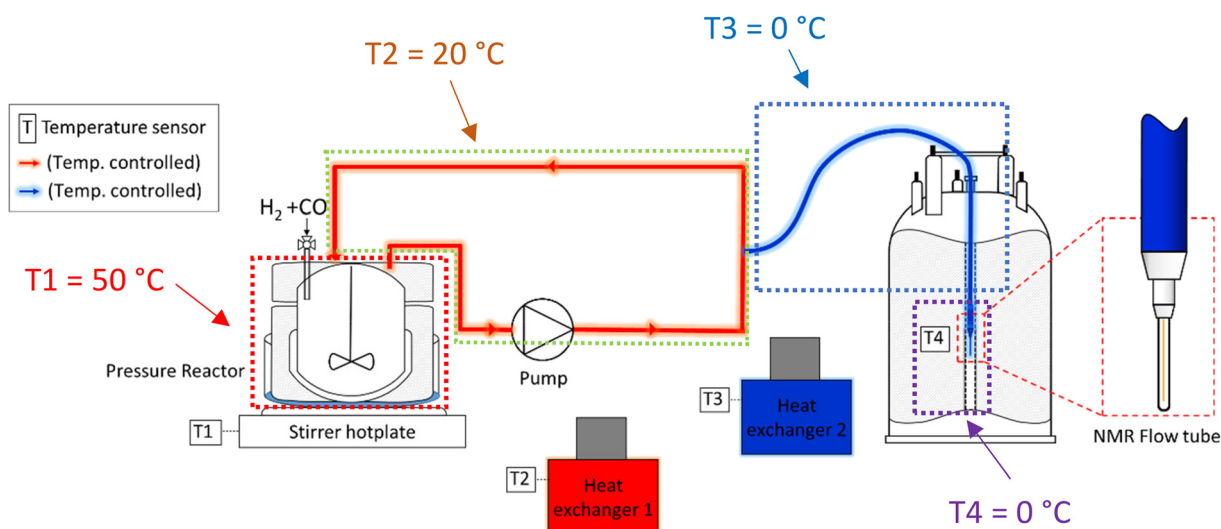
spectroscopy under 10–12 bar of H$_2$/CO (various ratios) at 50 °C (Fig. 4). These experiments were carried out as described in the ESI,† using 25 mL of non-deuterated toluene with rhodium concentrations of 2.5 mM and 1-hexene concentrations of 500 mM corresponding to a [S]/[Rh] = 200 or 0.5 mol% catalyst loading in all cases. The concentration of PPh$_3$ was varied from 0–250 mM resulting in ratios of [PPh$_3$]/[Rh] = 0–100.

**2.2.1 Quantitative FlowNMR analysis under isothermal conditions.** When two or more equivalents of PPh$_3$ per Rh were used, the only Rh–H species detected in the reaction mixture during turnover were **A/B** with no **C/D** observed in the $^{31}$P{$^1$H} and $^1$H FlowNMR spectra under the conditions applied (Fig. S6 and S7†). This observation reflects the competitive binding of dissolved CO against PPh$_3$ coordination even at higher ligand loadings. The amount of **A/B** increased sharply at the beginning of the catalysis (first 20 min) and then continued to grow more slowly throughout

the reaction as the rate of product formation slowed down (Fig. 6), suggesting the bis-PPh$_3$ hydrido-carbonyl complexes **A/B** to be an at-cycle resting state for the active hydroformylation catalyst generated *in situ* from [Rh(acac)(CO)$_2$]. A quantitative comparison at different ligand loadings showed a gradual shift of more Rh residing in **A/B** during catalysis the more PPh$_3$ was added, conditions that lead to slower hydroformylation (Fig. 6).

Interestingly, when only one equivalent PPh$_3$ was used in the reaction no Rh–H species were observed during catalysis, and the only catalyst intermediate detected by $^{31}$P{$^1$H} FlowNMR was the mono-phosphine acyl complex **Q** (Fig. S8†) identified previously.[28]

When the syngas composition was changed from 1:1 to 3:1 H$_2$/CO at the same total pressure in an experiment using six equivalents of PPh$_3$ the catalysis was ~30% faster (Fig. 6), reflecting the positive reaction order in H$_2$ which effects the turnover-limiting hydrogenolysis. CO is known to have a
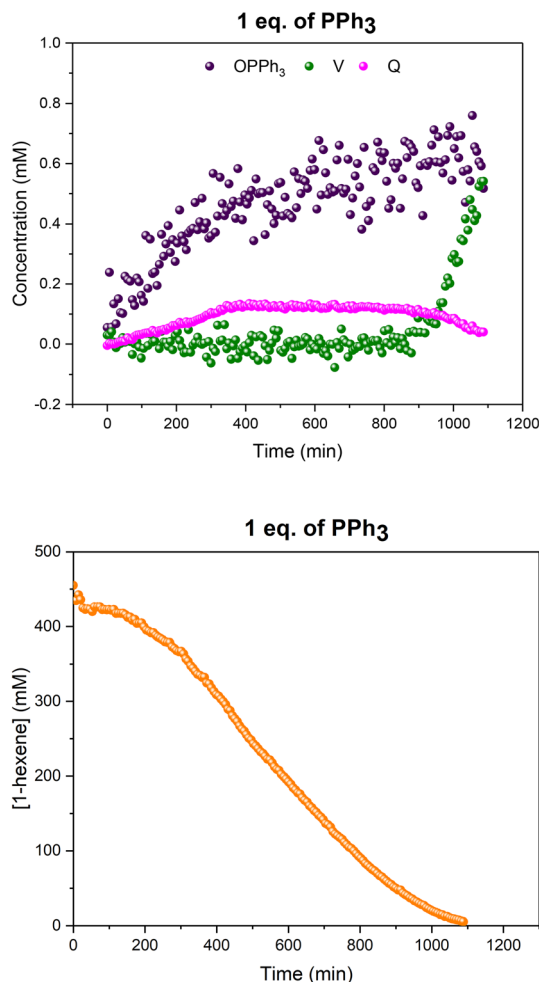


**Fig. 7** Schematic of the FlowNMR apparatus (not in scale) showing different temperature zones throughout the flow path.

**5506** | *Catal. Sci. Technol.*, 2022, **12**, 5501–5516

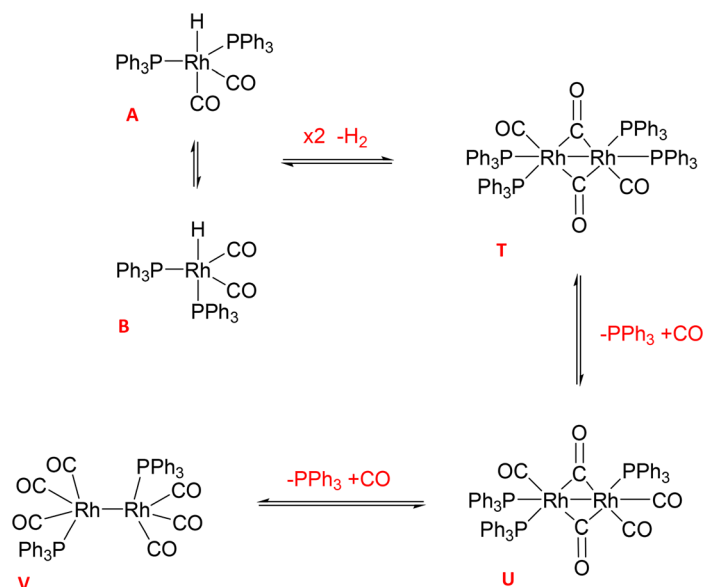This journal is © The Royal Society of Chemistry 2022

negative effect on the reaction kinetics, partially due to the formation of inactive dimers, trimers and other carbonyl species without hydrido groups, reducing the amount of active Rh–H complexes.[36] The amount of **A/B** detected with three times more $H_2$ over CO was increased (Fig. 6), showing a stepwise profile consisting of a steady-state plateau around 60% of all Rh while hydroformylation was rapid (15–75 min) followed by a gradual increase to 90% after the catalysis had ceased after 2.5 h (Fig. S9 and S10†).

While monitoring the amount of **A/B** delivered interesting insights into the catalyst speciation during turnover, the quantitative FlowNMR analysis was still missing a fraction of the Rh loading used. In addition to the possible formation of Rh-carbonyl clusters lacking any $^1H$ and $^{31}P$ NMR signature, the $^{31}P\{^1H\}$ NMR spectra did contain several weak signals with characteristic $^1J_{Rh-P}$ coupling, but due to the low S/N under the conditions applied (*i.e.* at sub-mM concentrations and 50 °C) and unknown $T_1^*$ values these could not be reliably characterised and quantified.

**2.2.2 Quantitative FlowNMR analysis using a controlled temperature gradient.** Typically, *operando* FlowNMR investigations are based on the idea of maintaining reaction conditions throughout the system (*i.e.* from reactor to magnet and back) in order not to disrupt the reaction and observe it in its true working state. The observation of dissolved $H_2$ in solution and detection of hydrido-carbonyl complexes that are unstable in the absence of excess syngas proved that this had been achieved in this case.[28] However, analysing the flowing sample by multi-nuclear FlowNMR spectroscopy at reaction temperature (50 °C in this case) means that only time-averages of all equilibria were detected by the relatively slow NMR acquisition. In addition, sensitivity is reduced at higher temperatures due to a less favourable Boltzmann distribution, as shown in section 2.1.2. We thus wondered whether a controlled temperature gradient between the reactor and the spectrometer could be applied,



**Fig. 8** Profiles of catalyst species from quantitative $^{31}P\{^1H\}$ FlowNMR (upper) and 1-hexene concentration from quantitative $^1H$ FlowNMR (lower) during the hydroformylation of 1-hexene under 10 bar of CO/$H_2$ (1:1) at 50 °C catalysed by [Rh(acac)(CO)$_2$] = 2.5 mM and [PPh$_3$] = 2.5 mM in 22.4 mL of non-deuterated toluene using the temperature gradients shown in Fig. 7.



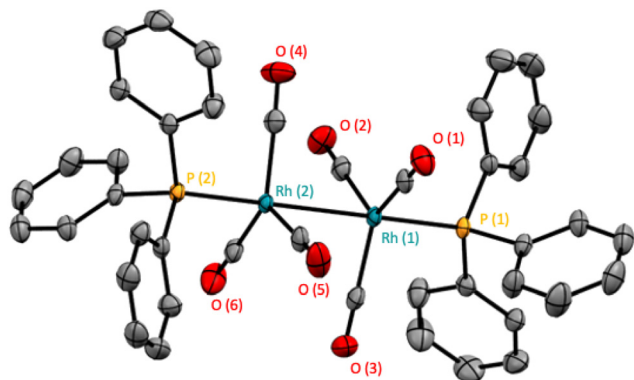**Scheme 3** Equilibria forming dimeric Rh$^0$ species from **A/B** *via* reductive coupling.

This journal is © The Royal Society of Chemistry 2022

*Catal. Sci. Technol.*, 2022, **12**, 5501–5516 | 5507

**Fig. 9** Solid-state structure of [Rh(CO)₆(PPh₃)₂] (**V**). Hydrogen atoms have been omitted for clarity and thermal ellipsoids are shown at 50% probability level.

where a lower NMR detection temperature would retain all reactive intermediates but slow down their interconversion so they could be detected separately, with increased S/N. Given a reaction mass ratio of ~3:1 in favour of the reactor *versus* the flow system and average residence times of 1.6 min in the latter, the thermal effect on the reaction rate would be acceptable if a consistent temperature gradient was used throughout all experiments. With separate heating circuits for different sections of our FlowNMR setup[19] we thus applied a stepwise temperature gradient from 50 °C in the reactor down to 0 °C in the tip of the flow tube in the NMR spectrometer and back (Fig. 7).

The temperature of the sample arriving at the tip of the flow tube in the NMR probe under the conditions applied (4 mL min⁻¹ flow rate) was shown to be 7 °C using the methanol NMR thermometer[37] (Table S4†). Gratifyingly, the NMR signals of complexes **A**/**B** flowing through the system under these conditions exhibited the decoalescence observed
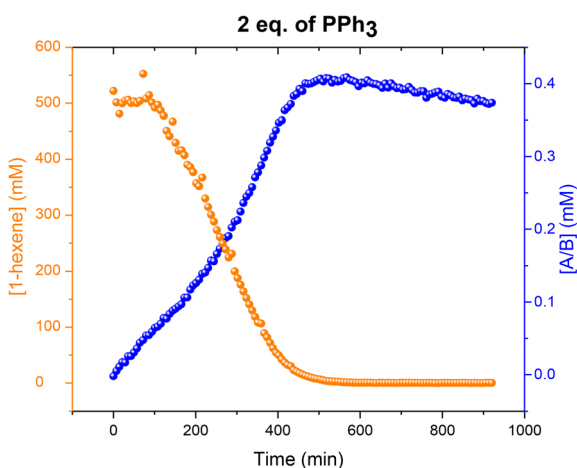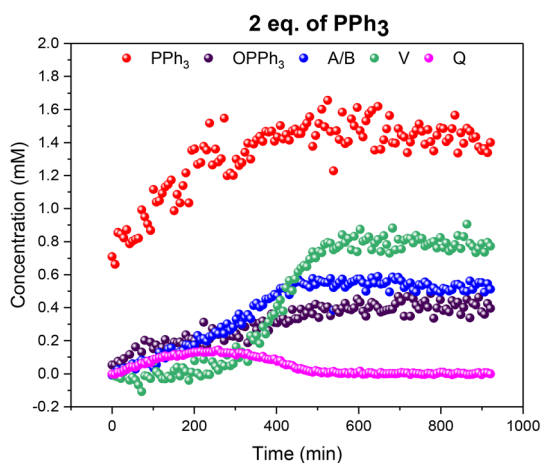




**Fig. 10** Profiles of catalyst species from quantitative ³¹P{¹H} FlowNMR (upper) and 1-hexene concentration from quantitative ¹H FlowNMR (lower) during the hydroformylation of 1-hexene under 10 bar of CO/H₂ (1:1) at 50 °C catalysed by [Rh(acac)(CO)₂] = 2.5 mM and [PPh₃] = 5 mM in 22.4 mL of non-deuterated toluene using the temperature gradients shown in Fig. 7.





**Fig. 11** Profiles of catalyst species from quantitative ³¹P{¹H} FlowNMR (upper) and 1-hexene concentration from quantitative ¹H FlowNMR (lower) during the hydroformylation of 1-hexene under 10 bar of CO/H₂ (1:1) at 50 °C catalysed by [Rh(acac)(CO)₂] = 2.5 mM and [PPh₃] = 7.5 mM in 22.4 mL of non-deuterated toluene using the temperature gradients shown in Fig. 7.

**5508** | *Catal. Sci. Technol.*, 2022, **12**, 5501–5516

This journal is © The Royal Society of Chemistry 2022

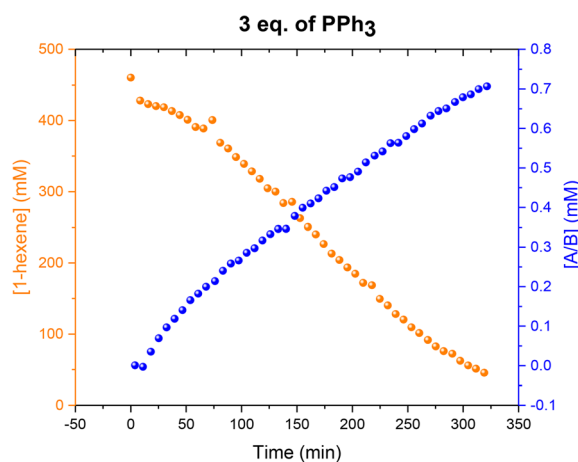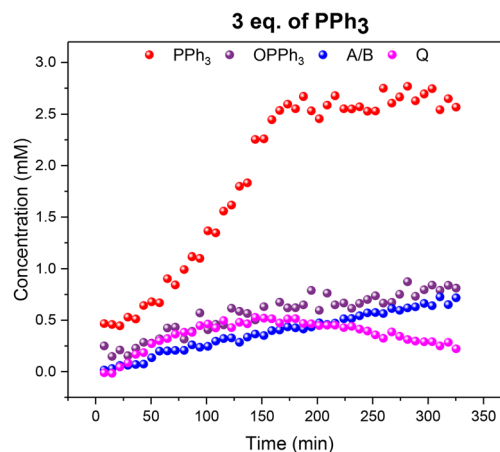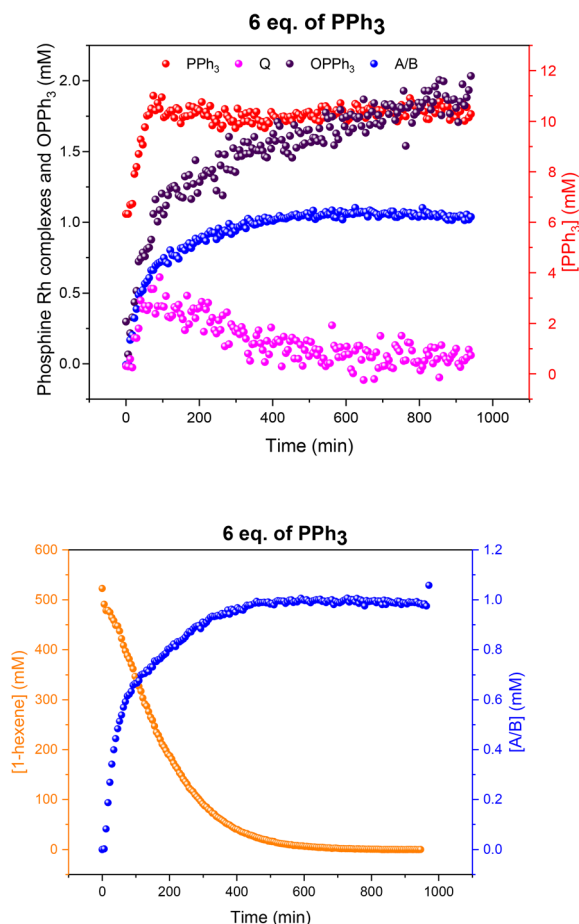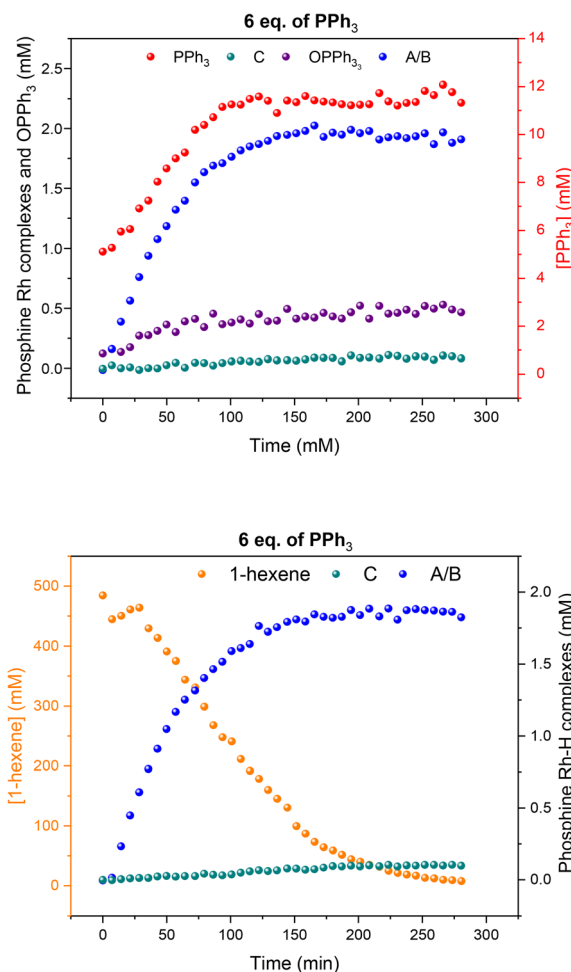**Fig. 12** Profiles of catalyst species from quantitative $^{31}P\{^1H\}$ FlowNMR (upper) and 1-hexene concentration from quantitative $^1H$ FlowNMR (lower) during the hydroformylation of 1-hexene under 10 bar of CO/H$_2$ (1:1) at 50 °C catalysed by [Rh(acac)(CO)$_2$] = 2.5 mM and [PPh$_3$] = 15 mM in 22.4 mL of non-deuterated toluene using the temperature gradients shown in Fig. 7.



**Fig. 13** Profiles of catalyst species from quantitative $^{31}P\{^1H\}$ FlowNMR (upper) and 1-hexene concentration from quantitative $^1H$ FlowNMR (lower) during the hydroformylation of 1-hexene under 10 bar of CO/H$_2$ (1:3) at 50 °C catalysed by [Rh(acac)(CO)$_2$] = 2.5 mM and [PPh$_3$] = 15 mM in 22.4 mL of non-deuterated toluene using the temperature gradients shown in Fig. 7.

in VT-NMR experiments performed in NMR tubes (Fig. S1 and S2 and S10 and S11†), and the $^{31}P\{^1H\}$ S/N increased almost nine-fold from 3.2 at 50 °C to 27.8 at 7 °C.
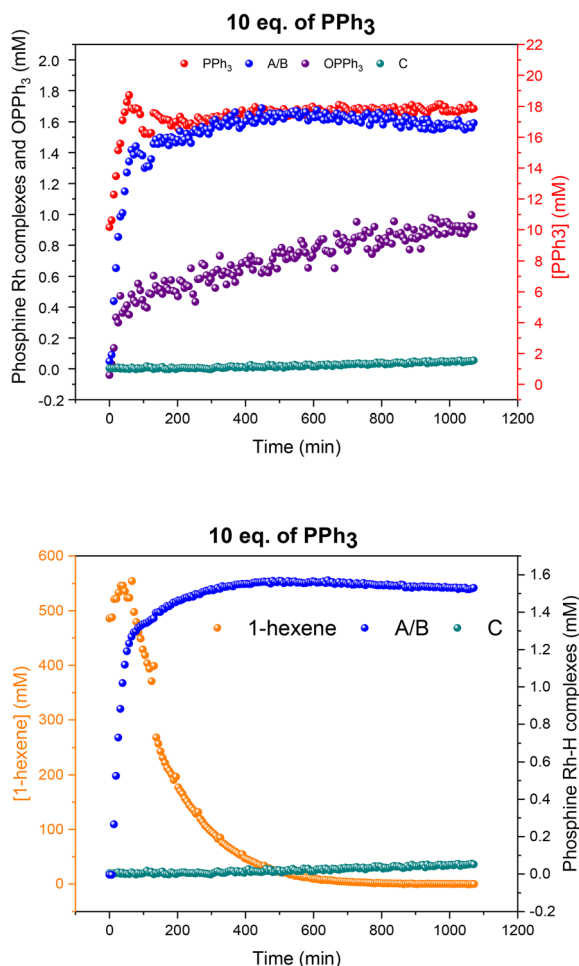
When hydroformylation catalysis with one equivalent of PPh$_3$ per Rh was monitored using this controlled temperature gradient (Fig. 7), the mono-phosphine acyl complex **Q** was the only Rh complex detected during turnover (Fig. 8), as in the experiments at constant 50 °C. More detailed analysis using a $D_1$ of 35 seconds showed the existence of both linear and branched acyl isomers of **Q** (Fig. S12†).

As can be seen from the $^{31}P\{^1H\}$ NMR profiles shown in Fig. 8 a noticeable amount of triphenylphosphine oxide was also formed during the reaction, as also seen in all other experiments with this catalytic system (see below). Control reactions in thoroughly deoxygenated and sealed sample tubes showed this to be an intrinsic feature of the catalysis, and not due to traces of oxygen being present within or penetrating the flow system over time. Furthermore, a significant proportion of the Rh used was not detected by

quantitative $^1H$ and $^{31}P\{^1H\}$ NMR spectroscopy under these conditions, suggesting the formation of a significant amount of Rh-carbonyl clusters when using one equivalent of PPh$_3$.
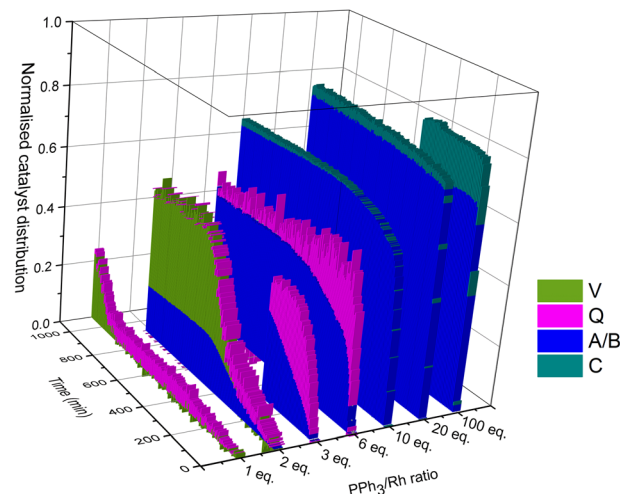
With the increased resolution and sensitivity at lower sample temperature, a new Rh–P species was detected towards the end of the reaction once substrate concentration had fallen below 50 mM. A signal centred at 27.8 ppm with second order coupling including a $^1J_{Rh–P}$ = 136 Hz (Fig. S12 and S13†) was identified as the carbonyl phosphine Rh dimer [Rh(CO)$_6$(PPh$_3$)$_2$] **V** (Scheme 3). This compound has previously been reported by Bianchini et al. who suggested the structure of the dimer to have two μ(CO) groups bridging the metals without a formal metal–metal bond.[9] However, single crystal X-ray diffraction of a sample of **V** synthesised through the reaction of [Rh(acac)(CO)(PPh$_3$)] with syngas showed it to possess three terminal carbonyls on each metal in staggered arrangement around a Rh–Rh single bond of 2.812 Å (Fig. 9).

This journal is © The Royal Society of Chemistry 2022

Catal. Sci. Technol., 2022, **12**, 5501–5516 | **5509**

**10 eq. of PPh₃**



**10 eq. of PPh₃**

**Fig. 14** Profiles of catalyst species from quantitative $^{31}P\{^1H\}$ FlowNMR (upper) and 1-hexene concentration from quantitative $^1H$ FlowNMR (lower) during the hydroformylation of 1-hexene under 10 bar of CO/H₂ (1 : 1) at 50 °C catalysed by $[Rh(acac)(CO)_2]$ = 2.5 mM and $[PPh_3]$ = 25 mM in 22.4 mL of non-deuterated toluene using the temperature gradients shown in Fig. 7.

When two equivalents of PPh₃ per Rh were used **A/B** was still the only Rh–H complex detected throughout the reaction, as seen at constant 50 °C (Fig. S7 and S8†), but small amounts of the mono-phosphine acyl complex **Q** and the carbonyl phosphine Rh dimer **V** (Fig. S14†) were also detected using the low temperature flow acquisition (Fig. 10). Comparing the catalyst distribution profile with the reaction progress, two interesting observations can be made: (i) the build-up of the hydrido-phosphine resting state **A/B** mirrored substrate consumption (Fig. 10); and (ii) the decay of the in-cycle acyl intermediate **Q** aligned with the increase in dimer **V** at the end of the catalysis (from ~400 min). The slow, gradual decrease in **A/B** after full conversion produced more **V** *via* reductive coupling[9] (Scheme 3). The still incomplete mass balance and detection of free PPh₃ suggests that even under these conditions up to 70% of the Rh resided in phosphine-free Rh-carbonyl clusters during the reaction.



**Fig. 15** Comparison of Rh speciation over time during the hydroformylation of 1-hexene under 10 bar of CO/H₂ (1 : 1) at 50 °C catalysed by $[Rh(acac)(CO)_2]$ = 2.5 mM with varying amounts of PPh₃ in toluene as derived from quantitative FlowNMR spectroscopy.

When using three equivalents of PPh₃ per Rh, **Q** and **A/B** were again the main catalyst species observed throughout the reaction, with the appearance dimer **V** at the expense of in-cycle **Q** once the substrate had been consumed (Fig. 11). The build-up of the at-cycle hydrido-phosphine complexes **A/B** again mirrored substrate consumption, but with three equivalents of PPh₃ a small amount of a new Rh species was detected at 23.7 ppm ($^1J_{Rh–P}$ = 157 Hz) and 22.1 ppm ($^1J_{Rh–P}$ = 127 Hz) in the $^{31}P\{^1H\}$ NMR spectra (Fig. S15†) which was characterised as the tris-PPh₃ Rh-carbonyl dimer **U** (Scheme 3). The solid-state structure of **U** was also confirmed by X-ray crystallography on a post-reaction sample that confirmed the dimer structure with two μ(CO) groups between the metals as reported previously.[38]

Increasing the ligand loading to six equivalents under otherwise identical reaction conditions caused a similar profile of **A/B** during the catalysis, with increasing amounts as the reaction progressed to completion (Fig. 12) to reach 1 mM (40% of all Rh) after 8 hours. With an excess of free PPh₃ present the bis-phosphine hydrido complex **A/B** was stable without any detectable dimer formation during turnover. Due to the excess CO still present in solution, no tris-phosphine hydrido complex **C/D** was observed to form either. As with lower ligand loadings, a transient trace of the in-cycle acyl intermediate **Q** was present during turnover that reached a maximum of 0.5 mM (20% of all Rh) when the rate of the catalysis was highest, then decaying to **A/B** as the reaction approached completion. Only traces of dimers **U**

‡ Although supplied at a nominal purity of >97%, we always detected various amounts of PPh₃ oxide and dimer **R** in toluene solutions of commercial **C**, even when handled under strict air-free conditions. Although not directly observed, we also suspect the presence of some PPh₃-free Rh-carbonyl clusters in commercial samples of $[RhH(CO)(PPh_3)_3]$.

**5510** | *Catal. Sci. Technol.*, 2022, **12**, 5501–5516
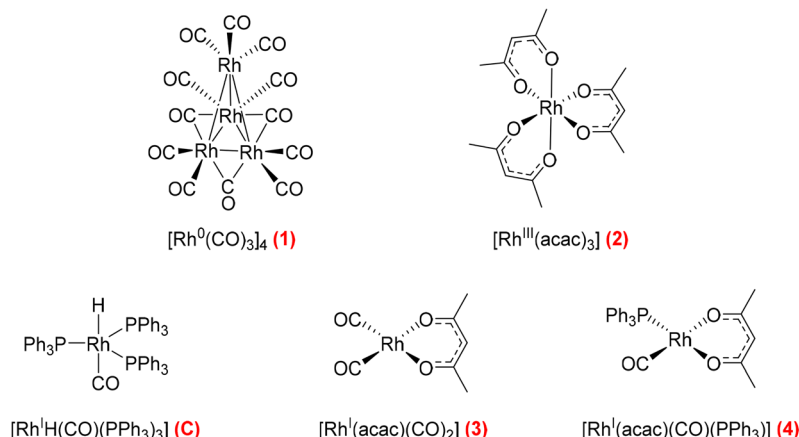
This journal is © The Royal Society of Chemistry 2022

**Fig. 16** Commercial Rh complexes commonly used as hydroformylation precursors investigated for their activation behaviour with $PPh_3$ and syngas in toluene.

and **V** were observed by $^{31}P\{^1H\}$ NMR after 16 hours under reaction conditions (Fig. S16 and S17†).

When changing the $H_2/CO$ ratio from 1:1 to 3:1 with six equivalents of $PPh_3$, hydroformylation catalysis was 40% faster with qualitatively the same trace of **A/B** over time (Fig. 13). With more $H_2$ present no acyl intermediate **Q** was observed during turnover, but a small amount of the tris-phosphine hydrido complex **C/D** formed under these CO-lean conditions. Both **A/B** and **C/D** were found to be stable under these conditions with no detectable amounts of dimers **U** or **V** in the $^{31}P\{^1H\}$ NMR spectra (Fig. S18†). Correspondingly, the concentrations of the at-cycle resting states **A/B** + **C/D** reached up to 2.4 mM (>95% of all Rh) towards the end of the reaction, evidencing negligible Rh-carbonyl cluster formation under these conditions.

Using 10 equivalents of $PPh_3$ per Rh with 1:1 syngas the catalysis was 10% slower than with 3–6 equivalents (see also Fig. 5), and catalyst distribution was further pushed into the at-cycle complexes **A/B** with no traces of acyl intermediate **Q** detected (Fig. 14). As when using 6 equivalents of $PPh_3$ and 3:1 $H_2/CO$ (Fig. 13), the phosphine hydrido complexes were stable towards dimerization to **U** or **V** with 10 equivalents of $PPh_3$ but only made up 1.6 mM (65% of all Rh) indicating the formation of some $^1H$ and $^{31}P$ NMR silent Rh-carbonyl clusters.

All these trends continued when increasing the ligand loading further to 20 and 100 equivalents of $PPh_3$ per Rh: the higher the excess of free ligand the slower the catalysis, and more **A/B** was pushed into **C/D** with no acyl intermediate **Q** or dimers **U** and **V** detected during the reaction (Fig. S19 and S20†).

Taking all this data together, quantitative catalyst maps can be built that illustrate the shift in Rh speciation across different conditions. Fig. 15 illustrates the evolution in speciation over reaction time using 1:1 $H_2/CO$ at 50 °C for ligand loadings of 1–100 equivalents. Any undetected Rh in this normalised plot either resides in Rh-carbonyl clusters or metallic Rh nanoparticles or deposits.

If the mechanistic relevance of at least the main catalyst species observed is known, such maps can be used to rationalise observations of catalyst activity and stability. In this case, hydroformylation catalysis was fastest with 3–6 equivalents of $PPh_3$, conditions that produced an observable amount of mono-phosphine acyl intermediate **Q** along with moderate quantities (<50% of all Rh) of the bis-phosphine hydrido complexes **A/B**. Conditions with less $PPh_3$ gave rise to more phosphine-carbonyl dimer **V** and large amounts of other, uncharacterised Rh-carbonyl clusters, leading to lower hydroformylation activity. Using >6 equivalents of $PPh_3$ on the other hand decreased the amount of carbonyl dimers and clusters to shift the Rh distribution more into the bis-phosphine hydrido complex



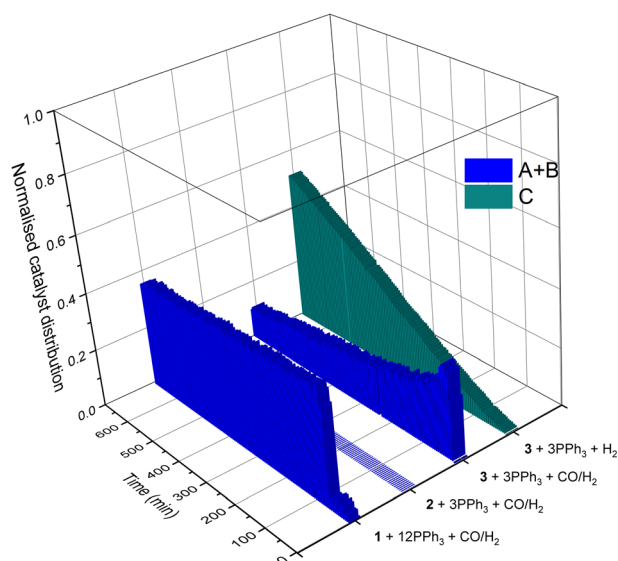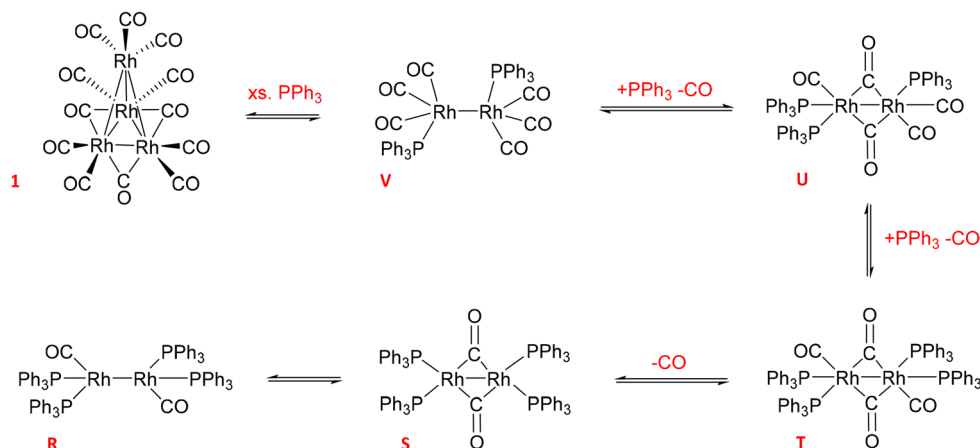**Fig. 17** Activation of different Rh precursors (Fig. 16) at 2.5 mM in toluene with $PPh_3$ and $H_2$ and/or CO at 10 bar and 50 °C as derived from quantitative FlowNMR spectroscopy.

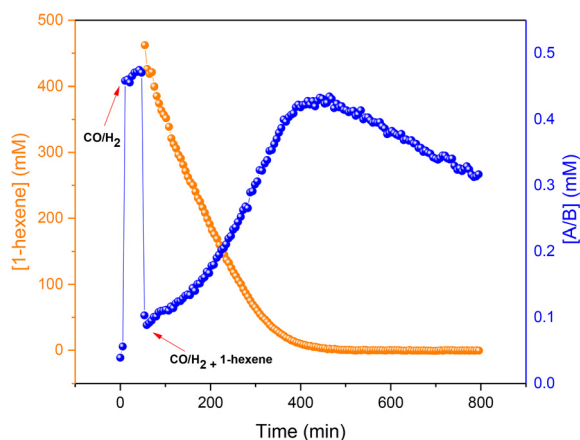This journal is © The Royal Society of Chemistry 2022

*Catal. Sci. Technol.*, 2022, **12**, 5501–5516 | **5511**

**Scheme 4** Equilibria of Rh$^0$ dimer formation from [Rh$_4$(CO)$_{12}$] with PPh$_3$ and CO in toluene (covalent Rh–Rh interactions render the d$^9$ systems diamagnetic and thus NMR active).

**A/B,** thereby also slowing down the rate of the catalysis. The optimum performance with 3–6 equivalents of ligand can thus be understood as the best compromise between under- and over-coordination of Rh by PPh$_3$ versus the substrates CO, H$_2$ and alkene. Increasing the H$_2$/CO ratio can increase catalyst activity further by lowering the amount of competitive carbonyl binding that decreases the rate (see Fig. 13). Changes in concentration, pressure, temperature, ligand and substrate are all expected to shift these effects due to the highly dynamic nature of the catalyst system, but as long as the key intermediates can be detected and reliably quantified the behaviour of the catalytic system may be mapped out in the same way. In the following we briefly investigate precursor activation and catalyst stability in the absence of substrate with the same approach.
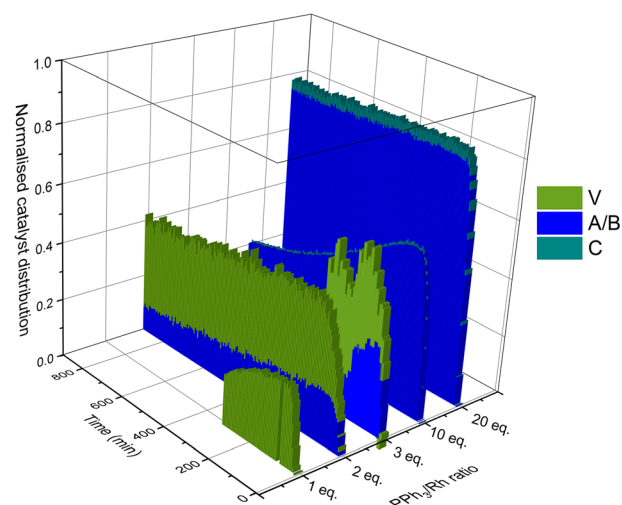
**2.2.3 Precursor activation.** In all previous experiments the activation of the [Rh(acac)(CO)$_2$] precursor was carried out *in situ* in the presence of 1-hexene, meaning that activation and hydroformylation catalysis started simultaneously as soon as H$_2$ and CO were added to the autoclave. Although no significant lag phases in product formation were observed under these conditions, the rise in the formation of the hydrido-phosphine complexes over the first 20–30 minutes of the reaction indicated that precursor activation was perhaps not instantaneous.

Various pre-activation protocols aimed at maximising initial rates have been used in the hydroformylation literature.[39,40] Most studies adopt the common practice of exposing the Rh precursor and ligand to syngas for several hours with heating before the autoclave is vented, substrate added and repressurised with syngas to start the hydroformylation reaction. However, the different precursors, solvents, ligands and conditions used in these



**Fig. 18** Profiles of **A/B** and substrate during the hydroformylation of 1-hexene under 10 bar of CO/H$_2$ (1:1) at 50 °C starting with [**C**] = 2.5 mM in 22.4 mL of non-deuterated toluene as derived from quantitative FlowNMR.



**Fig. 19** Concentration profiles of hydrido phosphine Rh complexes for the reaction of [**2**] = 2.5 mM with various equivalents of PPh$_3$ in 22.4 mL of non-deuterated toluene under 10 bar of CO and H$_2$ at 50 °C as derived from quantitative FlowNMR spectroscopy.

pre-activation protocols make rationalisation of the effectiveness of these procedures difficult. We thus decided to map the activation and stability of some commercial Rh precursors commonly used for hydroformylation catalysis using quantitative FlowNMR spectroscopy (Fig. 16).

Following the speciation of 1–4 under various activating conditions over time with quantitative $^1H$ and $^{31}P\{^1H\}$ FlowNMR spectroscopy yielded insight into the effectiveness of the different precursors and activation protocols. All precursors except 2 reacted with PPh$_3$ and syngas to give hydrido-phosphine complexes for hydroformylation catalysis (Fig. 17). Even after 12 hours with three equivalents of PPh$_3$ under 10 bar H$_2$/CO at 50 °C the tris-acac Rh$^{III}$ complex 2 had not formed any detectable Rh–P or Rh–H species, and the sharp $^{31}P\{^1H\}$ NMR peak of free PPh$_3$ indicated no chemical exchange with the Rh centre (Fig. S21†), showing 2 to be an unsuitable precursor under these relatively mild reaction conditions.

The reaction of 1 with 12 equivalents of PPh$_3$ (three per Rh atom) under Ar produced a mixture of the previously detected dimer U (Scheme 4) as well as the known Rh phosphine dimers R (37.5 ppm with $^1J_{Rh-P}$ = 196 Hz) and S (17.2 ppm with $^1J_{Rh-P}$ = 155 Hz) (Fig. S22†).[9] All of these formed by PPh$_3$/CO displacement and rearrangement, redox-neutral processes which are deemed fully reversible under the conditions applied (Scheme 4).

Adding 10 bar syngas to this mixture triggered the formation of A/B to up to 40% of all Rh in solution within 30 minutes at 50 °C, which were stable in toluene over >10 hours (Fig. 17). Venting the syngas at the end of the experiment showed traces of C/D and reformation of some dimer U in the mixture under Ar (Fig. S23–S27†). After re-pressurising the solution with 10 bar of CO C/D completely disappeared to only show A/B together with the carbonyl-rich dimers U and V (Fig. S24†), further evidencing their reversible interconversion (Scheme 4).

To assess the stability of the preformed hydrido complex C, it was pressurised with 10 bar 1:1 CO/H$_2$ at 50 °C without additional PPh$_3$. Notably, even before applying syngas only 70% of the nominal Rh loading was detected as C/D in toluene solution.‡ Immediately after adding 10 bar CO/H$_2$ about 40% was transformed into A/B through PPh$_3$ substitution by CO, and the mixture remained stable for at least one hour at 50 °C in toluene. Addition of 1-hexene and re-pressurisation with syngas gave rise to the hydroformylation activity expected under these conditions (Fig. 11) that saw A/B dropping sharply at the start of the catalysis and then building up again towards the end of the reaction (Fig. 18) after which it started decaying to dimers U and V.

This behaviour showed that starting with precursor C or even pre-activating it with syngas to A/B is not necessary, as the same reactivity may be obtained starting from 3 or 4 with added PPh$_3$ (Fig. 8). On the contrary, the latter

experiment even gave slightly higher rates (~15%) than the former, probably due to some decomposition of C during the pre-activation process in the experiment shown in Fig. 18.

Additional evidence for the formation of inactive Rh-carbonyl clusters from A/B and/or C/D under CO-rich and substrate-lean conditions came from an experiment studying C under 10 bar of carbon monoxide. Immediately after pressurising with the solution with CO C completely disappeared from the $^{31}P\{^1H\}$ NMR spectra, but only 10% of the Rh used was detected as A/B (Fig. S28†) alongside traces of dimers U and V (Fig. S29 and S30†).

The reaction of the widely used precursor 3 with three equivalents of PPh$_3$ under 10 bar of CO and H$_2$ at 50 °C (our typical hydroformylation conditions) quickly yielded A/B in a maximum amount of 30% of all Rh added within 30 min (Fig. 17). As previously observed during catalysis, no C/D was detected under syngas due to the excess of CO present. In the absence of substrate, the amount of A/B formed from 3 under these conditions started to fall to reach 10% of all Rh after 12 hours, forming small amounts of dimer V by way of reductive coupling (Scheme 3). The up to 70% of undetected Rh presumably resided in $^{31}P\{^1H\}$ NMR-silent Rh-carbonyl clusters under these conditions (Fig. S32†). When the autoclave was vented at the end of the experiment and repressurised with 10 bar of H$_2$ the tetra-phosphine dimer T was observed at the expense of the tris-phosphine dimer V, confirming their interconversion via PPh$_3$/CO exchange (Fig. S33†). Although these H$_2$-rich conditions did not lead to the reformation of A/B from the Rh$^0$ dimers, the addition of 1-hexene followed by 10 bar of CO/H$_2$ to this sample started hydroformylation catalysis with the disappearance of all dimeric species and formation of the acyl complex Q as observed previously (Fig. S34† and 11). However, although the reaction was 30% slower (Fig. S35†), this observation clearly establishes the reversibility of the formation of these Rh$^0$ dimers, meaning that they too are at-cycle catalyst resting states that may liberate active species via A/B under favourable conditions (Scheme 3). When the activation of 3 with three equivalents of PPh$_3$ was followed under 10 bar of H$_2$ the reaction proceeded more slowly to form the tris-phosphine hydrido complexes C/D up to a maximum of 55% of all Rh after 12 hours due to the absence of excess CO (Fig. S36 and S37†). Using two equivalents of PPh$_3$ with 3 under 10 bar of H$_2$ yielded a mixture of A/B and C/D that peaked at 20% of all Rh after 3.5 hours at 50 °C after which it decayed to <5% after 12 hours (Fig. S38†).

Following the activation of 3 under 10 bar of CO and H$_2$ in the presence of various amounts of PPh$_3$ (Fig. S39–S45†) showed a shift in Rh speciation similar to catalytic turnover conditions (Scheme 4): the less PPh$_3$ was used the more dimer V was formed, with more PPh$_3$ leading

This journal is © The Royal Society of Chemistry 2022

*Catal. Sci. Technol.*, 2022, **12**, 5501–5516 | **5513**

to a gradual shift to **A/B** and eventually some **C/D** (Fig. 19). With PPh$_3$ loadings of <10 these pre-activated mixtures slowly decomposed to uncharacterised Rh-carbonyl clusters over the course of several hours at 50 °C, but using 20 or more equivalents of PPh$_3$ yielded stable mixtures that did not deteriorate over at least 10 hours. Comparing the stability of **A/B** in the absence (Fig. 19) and presence (Fig. 15) of substrate showed hydroformylation catalysis to delay the decay by engaging more of the Rh in in-cycle species during turnover.

**2.2.4 Catalyst stability.** When analysing the $^{31}$P{$^1$H} NMR spectra of samples of **C/D** that had been heated to 50 °C in toluene for multiple hours, characteristic resonances[41] for bridging Rh–PPh$_2$–Rh phosphide units were detected at 190 ppm (Fig. S47†) alongside with the appearance of benzene in the $^1$H NMR spectra. Heating the sample to 90 °C for 1 h under Ar caused the appearance of multiple new $^{31}$P NMR resonances with complicated, higher order coupling patterns (Fig. S48†) as well as multiple new hydride peaks in the $^1$H NMR spectra alongside a colour change from orange to dark brown. $^{31}$P–$^1$H HMBC NMR experiments showed cross peaks between several of these signals indicating the formation of various hydrido-phosphide clusters (Fig. S49†). These observations clearly show even the relatively stable tris-phosphine complex **C** to be prone to decomposition in dilute solution under inert conditions at temperatures as low as 50 °C.

When the experiment was repeated under 5 bar of syngas **A/B** was observed to form together with several peaks due to decomposition (Fig. S50 and S51†) but different and less abundant than those seen under argon. Characteristic phosphorus resonances at 180 ppm correlating with hydride signals at −9.9 ppm (Fig. S52†) indicated the formation of Rh–PPh$_2$–Rh hydrido clusters with different CO/PPh$_3$ ratios than those formed in the absence of syngas. Repeating the experiment in the presence of a large excess of PPh$_3$ (300 equivalents) showed no decomposition of **C** after heating to 90 °C (Fig. S53 and S54†), suggesting the decomposition to occur *via* dissociation of PPh$_3$ and formation of tetracoordinated Rh complexes as those proposed to lead into the catalytic hydroformylation cycle.

## 3 Conclusion

The results of this investigation have extended the use of multi-nuclear high-resolution FlowNMR spectroscopy to quantify catalytic intermediates in systems that engage in multiple equilibria and where the chemical exchange between different species is fast. Being able to quantify catalytic intermediates during catalytic turnover (*operando* conditions) allows to map out catalyst speciation over a range of conditions which may be used to guide process development and upscaling with optimal use of the precious catalyst. Key to this was the ability to apply a controlled temperature gradient that slowed down the fast interconversion of catalytic reaction intermediates and thus facilitated their characterisation and quantification by FlowNMR spectroscopy due to refined coupling patterns and increased signal-to-noise without disrupting the catalytic cycle. In general terms, this work has shown that:

a) *intra*molecular interconversion of stereoisomers does not affect NMR signal quantification;

b) *inter*molecular exchange between different species may impact observed $T_1$ values and thus potentially affect NMR signal quantification;

c) lower temperatures give higher signal intensities as well as shorter $T_1$;

d) with suitable acquisition parameters (accounting for the range of possible $T_1$ values) and appropriate internal standards, absolute $^{31}$P NMR spectroscopic quantification of dynamic reaction intermediates is possible in continuous flow.

In the case of the Rh/PPh$_3$ catalysed hydroformylation of 1-hexene, this approach has led to the successful investigation of the interconversion of [RhH(CO)(PPh$_3$)$_3$] (**C**), [RhH(CO)$_2$(PPh$_3$)$_2$] (**A/B**), [Rh{CO(CH$_2$)$_5$(CH$_3$)}(CO)$_3$(PPh$_3$)] (**Q**), [Rh$_2$(CO)$_4$(PPh$_3$)$_4$] (**T**), [Rh$_2$(CO)$_5$(PPh$_3$)$_3$] (**U**), [Rh$_2$(CO)$_6$(PPh$_3$)$_2$] (**V**), and [Rh$_2$(CO)$_2$(PPh$_3$)] (**R/S**) during precursor activation and catalytic turnover to provide the following insights:

(i) the major Rh species in the presence of syngas and PPh$_3$ is the bis-phosphine hydrido complex **A/B** which is in equilibrium with the tris-phosphine hydrido complex **C**;

(ii) both complexes are at-cycle resting states that liberate active Rh species into the catalytic cycle under turnover conditions, but both are prone to the formation of a series of Rh$^0$ dimers **R/S/T/U/V** by reductive coupling (Schemes 2 and 3);

(iii) the formation of these dimers from the phosphine–hydrido Rh$^I$ complexes is reversible but also connected to the reversible formation of higher nuclearity Rh$^0$-carbonyl clusters such as [Rh$_4$(CO)$_{12}$] and [Rh$_6$(CO)$_{16}$] (Scheme 4) which are all off-cycle species that can make up to 90% of the Rh speciation under CO-rich conditions with low amounts of PPh$_3$;

(iv) CO-lean conditions disfavour these off-cycle dimers and clusters to liberate more Rh into active states (such as mono-nuclear hydrido complexes), in line with the negative impact of CO on the reaction kinetics;

(v) with PPh$_3$, ligand loadings of 3–6 equivalents provide the highest rates by balancing catalyst inhibition by CO and PPh$_3$ saturation, respectively;

(vi) the monophosphine acyl complex **Q** observed with low amounts of PPh$_3$ (<3 equivalents) is the only in-cycle catalytic intermediate detectable under turnover conditions by $^1$H and $^{31}$P NMR spectroscopy, suggesting the majority of product formation proceeds *via* mono-PPh$_3$ species within the catalytic cycle;

(vii) [Rh$^{III}$(acac)$_3$] is an unsuitable precursor for hydroformylation catalysis with 10 bar syngas at 50 °C but Rh$^I$ acac complexes activate quickly under these conditions so that no pre-activation is necessary;

**5514** | *Catal. Sci. Technol.*, 2022, **12**, 5501–5516

This journal is © The Royal Society of Chemistry 2022

(viii) irreversible catalyst deactivation proceeds *via* P–C bond cleavage in low-coordinate Rh–PPh$_3$ complexes to irreversibly give carbonyl and hydrido Rh–PPh$_2$–Rh species.

We hope the above findings will prove useful in the understanding and application of Rh/PR$_3$ catalysed hydroformylation chemistry, and that the methods developed will help to unravel other dynamic catalytic systems in the future.

## Conflicts of interest

RF is an employee of Evonik GmbH who operate industrial hydroformylation plants. The other authors declare no conflicts of interest.

## Acknowledgements

## References

1 H. Adkins and G. Krsek, *J. Am. Chem. Soc.*, 1949, **71**, 3051–3055.

2 O. Roelen, (Chemische Verwertungsgesellschaft Oberhausen m. b.H.) DE 849548, 1938 & 1952, US 2327066, 1943 *Chem. Abstr.*, 1944, **38**, 3631.

3 L. A. van der Veen, P. C. J. Kamer and P. W. N. M. van Leeuwen, *Organometallics*, 1999, **18**, 4765–4777.

4 Y. Yan, X. Zhang and X. Zhang, *J. Am. Chem. Soc.*, 2006, **128**, 16058–16061.

5 G. R. Stephenson, *Organometallic chemistry: The transition elements*, 1996.

6 R. Franke, D. Selent and A. Börner, *Chem. Rev.*, 2012, **112**, 5675–5732.

7 B. Cornils, *Org. Process Res. Dev.*, 1998, **2**, 121–127.

8 H.-W. Bohnen and B. Cornils, *Adv. Catal.*, 2002, **47**, 1–64.

9 C. Bianchini, H. M. Lee, A. Meli and F. Vizza, *Organometallics*, 2000, **19**, 849–853.

10 D. Evans, G. Yagupsky and G. Wilkinson, *J. Chem. Soc. A*, 1968, 2660–2665.

11 K. Noack, *Spectrochim. Acta, Part A*, 1968, **24**, 1917–1920.

12 W. R. Moser, C. J. Papile, D. A. Brannon, R. A. Duwell and S. J. Weininger, *J. Mol. Catal.*, 1987, **41**, 271–292.

13 R. B. King, A. D. King, M. Z. Iqbal and C. C. Frazier, *J. Am. Chem. Soc.*, 1978, **100**, 1687–1694.

14 C. Kubis, M. Sawall, A. Block, K. Neymeyr, R. Ludwig, A. Börner and D. Selent, *Chem. – Eur. J.*, 2014, **20**, 11921–11931.

15 R. Whyman, K. A. Hunt, R. W. Page and S. Rigby, *J. Phys. E: Sci. Instrum.*, 1984, **17**, 559–561.

16 I. T. Horváth, R. V. Kastrup, A. A. Oswald and E. J. Mozeleski, *Catal. Lett.*, 1989, **2**, 85–90.

17 D. A. Foley, A. L. Dunn and M. T. Zell, *Magn. Reson. Chem.*, 2016, **54**, 451–456.

18 A. M. R. Hall, J. C. Chouler, A. Codina, P. T. Gierth, J. P. Lowe and U. Hintermair, *Catal. Sci. Technol.*, 2016, **6**, 8406–8417.

19 A. Saib, A. Bara-Estaún, O. J. Harper, D. B. G. Berry, I. A. Thomlinson, R. Broomfield-Tagg, J. P. Lowe, C. L. Lyall and U. Hintermair, *React. Chem. Eng.*, 2021, **6**, 1548–1573.

20 A. M. R. Hall, R. Broomfield-Tagg, M. Camilleri, D. R. Carbery, A. Codina, D. T. E. Whittaker, S. Coombes, J. P. Lowe and U. Hintermair, *Chem. Commun.*, 2018, **54**, 30–33.

21 J. H. Vrijsen, I. A. Thomlinson, M. E. Levere, C. L. Lyall, M. G. Davidson, U. Hintermair and T. Junkers, *Polym. Chem.*, 2020, **11**, 3546–3550.

22 A. M. R. Hall, P. Dong, A. Codina, J. P. Lowe and U. Hintermair, *ACS Catal.*, 2019, **9**, 2079–2090.

23 A. M. R. Hall, D. B. G. Berry, J. N. Crossley, A. Codina, I. Clegg, J. P. Lowe, A. Buchard and U. Hintermair, *ACS Catal.*, 2021, **11**, 13649–13659.

24 D. B. G. Berry, A. Codina, I. Clegg, C. L. Lyall, J. P. Lowe and U. Hintermair, *Faraday Discuss.*, 2019, **220**, 45–57.

25 J. Y. Buser and A. D. McFarland, *Chem. Commun.*, 2014, **50**, 4234–4237.

26 A. Martínez-Carrión, M. G. Howlett, C. Alamillo-Ferrer, A. D. Clayton, R. A. Bourne, A. Codina, A. Vidal-Ferran, R. W. Adams and J. Burés, *Angew. Chem., Int. Ed.*, 2019, **58**, 10189–10193.

27 A. C. Brezny and C. R. Landis, *ACS Catal.*, 2019, **9**, 2501–2513.

28 A. Bara-Estaun, C. Lyall, J. P. Lowe, P. G. Pringle, P. C. J. Kamer, R. Franke and U. Hintermair, *Faraday Discuss.*, 2021, **229**, 422–442.

29 U. Holzgrabe, I. Wawer and B. Diehl, *NMR Spectroscopy in Pharmaceutical Analysis*, Elsevier, 2008, pp. 43–62.

30 G. F. Pauli, B. U. Jaki and D. C. Lankin, *J. Nat. Prod.*, 2005, **68**, 133–149.

31 V. Rizzo and V. Pinciroli, *J. Pharm. Biomed. Anal.*, 2005, **38**, 851–857.

32 G. Helms, H. Dathe, N. Weiskopf and P. Dechent, *Magn. Reson. Med.*, 2011, **66**, 669–677.

33 C. Di Carluccio, M. C. Forgione, S. Martini, F. Berti, A. Molinaro, R. Marchetti and A. Silipo, *Carbohydr. Res.*, 2021, **503**, 108313.

34 R. Wei, C. L. Dickson, D. Uhrín and G. C. Lloyd-Jones, *J. Org. Chem.*, 2021, **86**, 9023–9029.

35 D. Camuffo, *Microclimate for Cultural Heritage*, Elsevier, 3rd edn, 2019, pp. 61–71.

36 V. K. Srivastava, S. K. Sharma, R. S. Shukla, N. Subrahmanyam and R. V. Jasra, *Ind. Eng. Chem. Res.*, 2005, **44**, 1764–1771.

This journal is © The Royal Society of Chemistry 2022

*Catal. Sci. Technol.*, 2022, **12**, 5501–5516 | 5515

37 M. Findeisen, T. Brand and S. Berger, *Magn. Reson. Chem.*, 2007, **45**, 175–178.

38 A. S. C. Chan, H.-S. Shieh and J. R. Hill, *J. Chem. Soc., Chem. Commun.*, 1983, 688–689.

39 A. A. Dabbawala, R. V. Jasra and H. C. Bajaj, *Catal. Commun.*, 2011, **12**, 403–407.

40 B. E. Hanson and M. E. Davis, *J. Chem. Educ.*, 1987, **64**, 928.

41 F. H. Jardine, *Polyhedron*, 1982, **1**, 569–605.

This journal is © The Royal Society of Chemistry 2022